

# Complex coacervation and compartmentalized conversion of prebiotically relevant metabolites

Iris B. A. Smokers<sup>‡[a]</sup>, Merlijn H. I. van Haren<sup>‡[a]</sup>, Tiemei Lu<sup>[a]</sup>, Evan Spruijt<sup>\*[a]</sup>

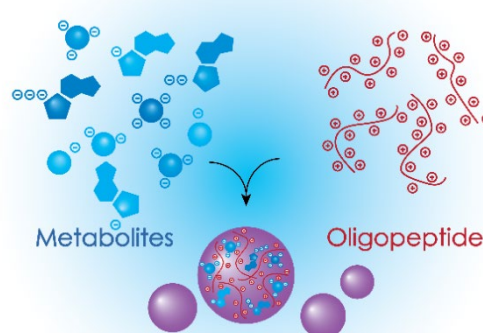
<sup>a</sup> Institute for Molecules and Materials, Radboud University, Heyendaalseweg 135, 6523 AJ Nijmegen, The Netherlands

<sup>‡</sup>These authors contributed equally. \* Corresponding author, e-mail: e.spruijt@science.ru.nl

**Keywords:** protocells, complex coacervation, compartmentalization, prebiotic chemistry

## Abstract

Metabolism and compartmentalization are two of life's most central elements. Constructing synthetic assemblies based on prebiotically relevant molecules that combine these elements can provide insight into the requirements for the formation of life-like protocells from abiotic building blocks. In this work, we show that a wide variety of small anionic metabolites have strong enough interactions with oligoarginine ( $R_{10}$ ) to form coacervate protocells through liquid-liquid phase separation. The stability of the coacervates can be rationalized by the molecular structure of the metabolites, and we show that three negative charges for carboxylates or two negative charges complemented with an unsaturated functional group for phosphates and sulfates is sufficient for phase separation. We show that these metabolites remain reactive in compartmentalized systems. Protometabolic reactions that lead to an increased interaction with the oligopeptide can be exploited to induce the formation of coacervate protocells. The resulting coacervates can localize other metabolites and enhance their conversion. Finally, reactions of compartmentalized metabolites can also alter the physicochemical properties of the coacervates and ultimately lead to protocell dissolution if the reaction products decrease the coacervate stability. These results reveal the intricate interplay between (proto)metabolic reactions and coacervate compartments, and show that coacervates are excellent candidates for metabolically active protocells.



## 28 Introduction

29 Metabolism and compartmentalization are fundamental elements of life.<sup>1, 2</sup> Prebiotic routes to form and  
30 convert central metabolites and ways to compartmentalize them are therefore of utmost relevance.  
31 Prebiotic reactions of common metabolites such as ATP, NADH and citric acid have been studied  
32 extensively, as these molecules play a key role across the tree of life in reaction pathways such as the  
33 tricarboxylic acid (TCA) cycle, which releases energy to fuel various cellular processes.<sup>3-9</sup> However, their  
34 concentrations on the early Earth were likely very low, slowing down these protometabolic reactions to  
35 non-viable pace. Moreover, some of the developed reactions proceed under mutually incompatible  
36 conditions of, for instance, pH, redox potential or light. Compartmentalization of reagents can increase  
37 local concentrations and create distinct chemical microenvironments, and might have therefore been an  
38 important step in gaining sufficiently high reaction rates and selectivity at the origins of life.<sup>10-13</sup>

39 Compartmentalization through self-assembly of amphiphiles into vesicles has long been  
40 considered as the general mechanism for the formation of the first protocells.<sup>14</sup> However, this  
41 encapsulation was likely inefficient without the presence of active exchange of components by complex  
42 transport machineries, limiting the local concentrations that could be reached inside these protocells.<sup>15</sup>  
43 Since the discovery that membraneless organelles in modern cells can form by liquid-liquid phase  
44 separation (LLPS), the analogous formation of protocells by LLPS has received increasing interest.<sup>16-18</sup>  
45 Multiple weak associative interactions, such as charge-charge and cation- $\pi$  interactions, between  
46 molecules can drive LLPS to form (complex) coacervates, which are droplets of a solute-rich phase  
47 dispersed in a dilute continuous phase.<sup>19, 20</sup> These coacervate protocells have been shown to  
48 spontaneously concentrate reagents and increase reaction rates,<sup>21, 22</sup> and recently it has been shown that  
49 they can even be formed by prebiotically relevant mononucleotides and short homopeptides containing  
50 just five residues.<sup>23, 24</sup> Moreover, droplets made from peptides with prebiotically relevant low molecular  
51 weight were found to be more effective at generating distinct pH microenvironments, accumulating RNA  
52 and stabilizing its secondary structure, than coacervates formed by high molecular weight  
53 polyelectrolytes.<sup>24</sup>

Since many key metabolites have multiple negative charges, we hypothesized that these metabolites could similarly undergo complex coacervation to become compartmentalized inside protocells, and that these protocells could be capable of sustaining metabolic reactions. While the large majority of complex coacervates in literature are composed of long polymers, a few examples of complex coacervates made of small metabolites have been reported. AMP and citric acid have been shown to phase separate with oligoarginine and protamine, a 4.2 kDa protein containing 21 arginine residues, respectively.<sup>24, 25</sup> Additionally, pyrophosphate and triphosphate were found to phase separate with lysozyme and histatin-5, both of which have a net charge of  $z = +6$  or  $+7$  at the investigated pH.<sup>26, 27</sup> However, a systematic analysis of phase separation of prebiotic metabolites is still lacking, and the metabolic activity of the coacervate protocells is unexplored.

Here, we show that anionic metabolites with at least three charges, or two when complemented with additional cation- $\pi$  or  $\pi$ - $\pi$  interaction sites, are able to form complex coacervates with the short peptide oligoarginine ( $R_{10}$ ). We compare various types of prebiotically relevant metabolites, including carboxylic acids, phosphates and sulfates in their ability to form coacervates, and show that their stability varies significantly due to small differences in molecular structures, such as their degree of unsaturation, hydrogen bonding ability and charge density. We show that these metabolites continue to undergo metabolic reactions and that these reactions can control compartmentalization and vice versa: metabolite conversion can give rise to active formation and growth of coacervate protocells, metabolite conversion can be accelerated inside coacervate compartments, and finally, metabolite conversion inside coacervates can alter the nature of the protocells, by creating products that affect the stability of the coacervates. These observations reveal the intricate interplay between protometabolic reactions and coacervate compartments, and show that coacervates are excellent candidates to compartmentalize protometabolic networks.

## Results and discussion

### Metabolites with at least two negative charges form stable coacervates with oligoarginine

Inspired by the central importance of metabolism in living systems, we wondered if key prebiotic metabolites could be compartmentalized by liquid-liquid phase separation, and if so, how propensity for phase separation is linked to the molecular structure. To answer these questions, we investigated three classes of metabolites and related small molecules: carboxylic acids, phosphates, and sulfite/sulfates. We selected di- and tricarboxylic acids from the tricarboxylic acid (TCA) and 4-hydroxy-2-ketoglutarate (HKG)<sup>4</sup> cycles, complemented with an aromatic tricarboxylic acid. Phosphates were selected that are part of the cellular respiration, like ATP, which functions as biochemical energy currency, or prebiotic analogues, such as triphosphate and trimetaphosphate (TMP). Finally, we selected sulfites and sulfates and some iron complexes, because of their possible relevance in protometabolic reactions on early Earth.<sup>28, 29</sup> For each molecule, we determined its ability to phase separate with a short oligoarginine peptide ( $R_{10}$ ). Oligoarginine was chosen as the model cation because it is known to form coacervates with small molecules like AMP and because arginine-containing peptides have been suggested to occur on the early Earth.<sup>24, 30</sup> To keep the system as simple as possible, stock solutions were adjusted to a pH of  $7.0 \pm 0.3$  with HCl and NaOH and no buffer was used, since excess ions present in the buffer can screen the electrostatic interactions and mask a potential phase separation. We decided to compare the ability of metabolites to form coacervates at equal concentration, so the concentration of all metabolites is fixed at 5 mM and  $R_{10}$  at 5 mM of arginine residues.

We found that carboxylic acid metabolites with three charges ( $z = -3$ ) were all able to form coacervate droplets with  $R_{10}$ , while monocarboxylic acids (MCA) and dicarboxylic acid (DCA) resulted in homogenous solutions (Table S1). For phosphates and sulfates, a similar trend is seen, as monophosphate ( $z = -2$ ) did not phase separate with  $R_{10}$ , whereas pyrophosphate ( $z = -3$ ) did. AMP and NADH were an exception and formed coacervates with  $R_{10}$  even though both molecules only have two negative charges. This can be explained by the cation- $\pi$  interactions of  $R_{10}$  with the nucleotide bases, which strengthen the overall intermolecular interactions between the metabolite and  $R_{10}$ , and is in agreement with previous

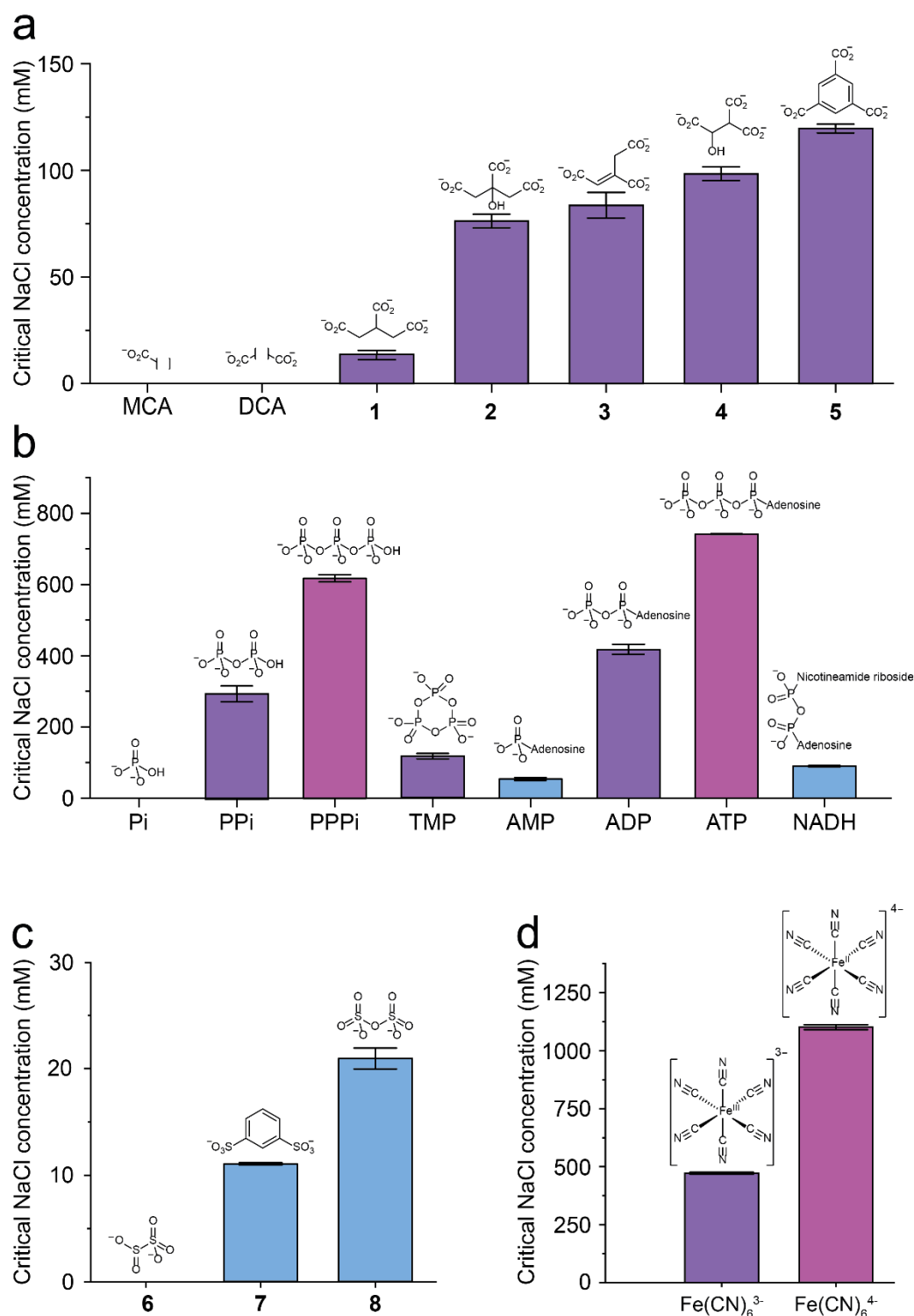


**Figure 1.** Critical salt concentrations of coacervate forming metabolites with oligoarginine. (a) Tricarboxylic acids phase separate with R<sub>10</sub> while monocarboxylic acid (MCA) and dicarboxylic acid (DCA) do not. (b) Phosphates containing two negative charges (blue) accompanied by a nucleobase can form coacervates with R<sub>10</sub>. (c) Sulfates with two negative charges form coacervates with R<sub>10</sub> while sulfites do not. (d) Ferri- and ferrocyanide coacervates have relatively high critical salt concentrations while not containing aromatic groups. Critical salt concentrations were determined by turbidity measurements and error bars represent the standard deviation ( $n = 3$ ). Empty regions between brackets indicate a variety of groups (Table S1). Concentration of all molecules is 5 mM (monomer units for R<sub>10</sub>) or 10 mM for sulfites and sulfates.

observations<sup>24</sup>. Interestingly, pyrosulfate (**8**) was also able to phase separate with R<sub>10</sub>, while having only two negative charges and no additional interacting groups. We attribute this to the high charge density and number of  $\pi$  electrons, which enhance pyrosulfate's ability to phase separate. Bisulfite did not phase separate with R<sub>10</sub>, which supports the hypothesis that the  $\pi$ -electrons in the oxygen sp<sup>2</sup> bond interacts with R<sub>10</sub> and contribute to phase separation.

To quantify the tendency of small metabolites to phase separate with cationic peptides, such as R<sub>10</sub>, we determined the critical salt concentration (CSC) for each coacervate by titrating the coacervate suspension with NaCl (Figure 1, Table S1). Differences in stability between different coacervate can be caused by the number and strength of interaction sites of their components.<sup>20</sup> For example, the guanidinium groups of R<sub>10</sub> form relatively strong charge-charge interactions with carboxylate groups compared to the cation- $\pi$  interactions they form with aromatic groups. The number of charged interaction sites will thus have a large effect on the overall coacervate stability, whereas an increase in cation- $\pi$  interactions will give a small increase in stability, and the ability to form hydrogen bonds an even smaller increase.<sup>20</sup> For the tricarboxylic acids, which all have three negatively charged groups, a higher CSC was found with an increasing number or strength of additional interaction sites (Figure 1a). For example, the additional hydroxyl group of citrate (**2**) and  $\pi$  bond of trans-aconitate (**3**) increased the CSC by 55 and 65 mM, respectively, compared to coacervates formed by R<sub>10</sub> and tricarballylate (**1**). Trimesate had the highest CSC of all tricarboxylic acid coacervates, which can be explained by the presence of the benzene ring that forms relatively strong cation- $\pi$  interactions with R<sub>10</sub> compared to the other additional interactions.<sup>20</sup>

For phosphate metabolites, a similar trend was observed: the CSC is determined in the first place by the number of negative charges, and secondly by additional interactions such as cation- $\pi$  interactions (Figure 1b). The CSC of R<sub>10</sub>/triphosphate (PPPi) coacervates was 300 mM higher than R<sub>10</sub>/pyrophosphate (PPi) coacervates due to the extra negatively charged phosphate group, whereas the CSC of R<sub>10</sub>/ATP coacervates was 100 mM higher than that of R<sub>10</sub>/PPPi coacervates because of the additional adenosine. Moreover, the CSC of R<sub>10</sub>/NADH coacervates was nearly double that of R<sub>10</sub>/AMP coacervates, demonstrating a nucleoside group can greatly increase coacervate stability. We also included

trimetaphosphate (TMP), which is a cyclic version of triphosphate and contains three negative charges. Interestingly, R<sub>10</sub>/TMP coacervates have a significantly lower CSC than R<sub>10</sub>/PPi coacervates (116.47 mM compared to 296.52 mM, respectively), while both molecules have the same net charge ( $z = -3$ ) and interacting groups. We attribute this decrease in coacervate stability to the lower flexibility of TMP compared to PPi, which reduces the number of dynamic interactions it can make with R<sub>10</sub>, an effect that has been observed in coacervates composed of polylysine and DNA.<sup>31</sup> When comparing the general stability of coacervates composed of phosphates compared to carboxylates, it becomes clear that the phosphate coacervates have higher CSCs at similar charge. This can possibly be explained by the higher charge density of the phosphates, as the anionic groups are not separated by an alkyl spacer like in tricarboxylic acids. An additional cause could come from their relative hardness (which manifests itself in a Hofmeister series), leading to a stronger hydration of phosphates.<sup>32</sup> Complex coacervation would release some of the bound water molecules, making phase separation with phosphates more favorable.

In the sulfite and sulfates section, it was found that R<sub>10</sub>/pyrosulfate (**8**) coacervates had a higher CSC than R<sub>10</sub>/1,3-benzenedisulfate (**7**) coacervates, which was surprising, as **7** contains an extra benzene group that forms cation- $\pi$  interactions with R<sub>10</sub> (Figure 1c). A possible reason for this could be the reduced flexibility of **7** compared to **8**, though it should be noted that a CSC difference of lower than 10 mM could have other causes and a wider range of compounds with varying charge densities should be used to determine the effect of molecular flexibility on electrostatic phase separation.

Lastly, it is striking how high the measured CSC of ferri- and ferrocyanide coacervates was compared other anions with three or four negative charges (Figure 1d). A reason for this could be that ferri- and ferrocyanide structurally contain six negative charges, which are countered by the ferric or ferrous cation to reach a net charge state of -3 and -4, respectively. This means that R<sub>10</sub> can effectively form more interactions with the iron complexes than with pyrophosphate, for example. Additionally, the  $\pi$ -electrons of the cyanide ligands could contribute to the coacervate stability by interacting with the sp<sup>2</sup> hybridized guanidinium group of arginine, while the lone pairs on the nitrogen can form hydrogen bonds. All these factors make ferri- and ferrocyanide coacervates incredibly stable compared to other small molecule coacervates.

Finally, it should be noted that the CSCs discussed here are determined from  $R_{10}$ /metabolite coacervates, and replacing  $R_{10}$  with a shorter polycation such as  $R_5$  would decrease the CSC of the coacervates or completely prevent LLPS from occurring.<sup>33</sup> In addition to  $R_{10}$ , we also investigated the stability of  $K_{10}$ /metabolite coacervates to determine the difference between arginine and lysine in complex coacervation (Table S1).  $K_{10}$  was not able to form coacervates with any of the tricarboxylic acids or sulfates used in this study. The CSCs of all  $K_{10}$ /phosphate coacervates were significantly lower than  $R_{10}$ /phosphate coacervates and TMP, AMP and NADH did not phase separate with  $K_{10}$  while they do with  $R_{10}$ . These results confirm the consensus that arginine has a higher propensity to phase separate as a result of the stronger cation- $\pi$  and additional  $\pi$ - $\pi$  interactions of arginine's guanidinium group compared to the amine group of lysine.<sup>24, 34, 35</sup> Taken together, these results show how metabolites can form stable coacervate protocells with a relatively short polycation.

#### **Active formation of coacervates by aldol addition**

We then asked if compartmentalization of these metabolites is compatible with their conversion by metabolic reactions, which is a prerequisite for a primitive metabolism in coacervate protocells. We expect that metabolism and coacervate compartments are mutually dependent: metabolic reactions could affect the coacervates by inducing phase separation or affecting their stability, but coacervates can also affect the rates of metabolism, analogous to the interplay between cellular processes and membraneless organelles.<sup>36,37</sup> Here, we show that conversion of metabolites can induce phase separation, that the conversion of metabolites can be enhanced inside coacervates, and that metabolic reactions taking place inside coacervates can affect their stability and ultimately lead to their dissolution.

Metabolic reactions of the compounds shown in Figure 1 can drive phase separation if the product of the reaction has stronger interactions with another species, such as  $R_{10}$ . Previous work has shown that the enzymatic conversion of ADP to ATP, which involves the introduction of an additional negative charge, can induce phase separation.<sup>38, 39</sup> Although the use of enzymes is far from prebiotically relevant, reactions involving the addition or removal of charged groups are ubiquitous in prebiotic pathways as well. Several reactions in the tricarboxylic acid (TCA) cycle and its prebiotic analogues introduce additional carboxylate



groups.<sup>4,5</sup> To determine whether such prebiotic reactions could give rise to active coacervate formation, we investigated the aldol addition reaction of 90 mM of the diacid malonate (**9**) with 120 mM glyoxylate (**10**) to form the triacid 3-carboxymalate (3-CM, **4**), shown schematically in Figure 2a.<sup>5</sup> 3-CM should be able to undergo LLPS with 5 mM R<sub>10</sub>, according to our results in Figure 1. Analysis by <sup>1</sup>H-NMR spectroscopy (Figure 2b, SI Figure S1) shows formation of 3-CM after 143 hours in a 22.8% yield. Similar yields were obtained in absence of R<sub>10</sub> (SI Figure S2-3). Nucleation of coacervate droplets could be seen after 59 hours under the microscope at a concentration of 11 mM 3-CM, after which the coacervate droplets continued to grow (Figure 2c, Supplementary Movie 1). Figure 2d shows the increase in average droplet size over time, which resembles previous observations of actively growing coacervate droplets.<sup>39</sup> A similar result was obtained for the aldol addition reaction between α-ketoglutarate and glyoxylate, which forms the tricarboxylic acids isocitroyl formate and aconitoyl formate (SI Figure S4-7). These results show that metabolite-containing coacervate protocells can be formed through prebiotically relevant metabolic conversions.

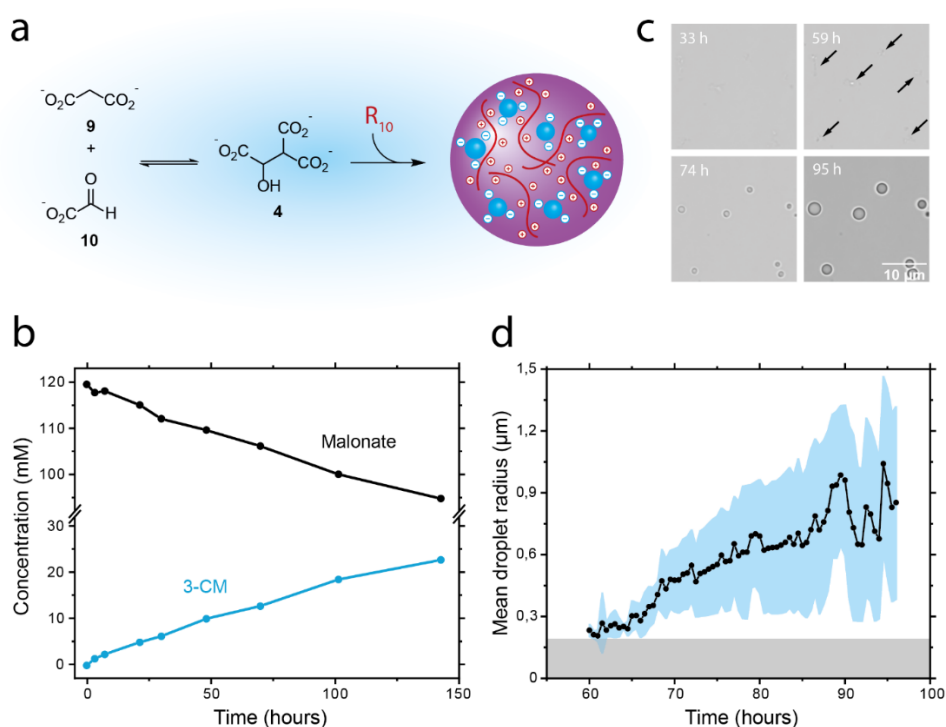


**Figure 2 Active formation of coacervates.** (a) Aldol addition reaction between dianion malonate (**9**) and glyoxylate (**10**) generates 3-carboxymalate (3-CM, **4**). The trianionic product can undergo LLPS with R<sub>10</sub>. (b) Plot of concentrations over time for the reaction of 90 mM disodium malonate with 120 mM sodium glyoxylate in the presence of 5 mM R<sub>10</sub> as observed by <sup>1</sup>H-NMR spectroscopy with 10 mM 3-(trimethylsilyl)propionic-2,2,3,3-d<sub>4</sub> acid sodium salt internal standard. (c) Brightfield microscopy images for the reaction of 90 mM disodium malonate with 120 mM sodium glyoxylate in the presence of 5 mM R<sub>10</sub>, showing the formation of coacervates as the reaction progresses. (d) Analysis of droplet size over time. Droplet area was converted to radius and mean droplet radius was calculated. Shaded areas indicate the standard deviation over all droplets in the frame (blue) and detection limit resulting from the threshold in droplet size analysis script (grey).

## Oxidation of NADH is enhanced inside coacervates

After the observation of coacervate formation by conversion of malonate to 3-CM, we investigated if the newly formed protocells could facilitate reactions involving metabolites. Recently, it was shown that simple coacervates can increase the rate of an aldol reaction<sup>18</sup>, which inspired us to investigate the influence of coacervates on a simple redox reaction. NADH was selected as reducing agent because of the prebiotic plausible synthesis and importance in metabolic networks,<sup>40, 41</sup> and the possibility to monitor it by fluorescence microscopy and absorbance. NADH was sequestered in the R<sub>10</sub>/3-CM coacervates formed in the previous section with a partitioning coefficient ( $K_p$ ) of  $91 \pm 4.6$ , meaning that the concentration inside the coacervate droplets is nearly two orders of magnitude higher than the supernatant (Figure 3a). We hypothesized that the locally increased concentrations inside coacervates can increase the rate of NADH-mediated reduction reactions (Figure 3b). We studied the conversion of NADH to NAD<sup>+</sup> by ferricyanide, an anionic oxidizing agent with a strong tendency to phase separate and a possible presence on prebiotic Earth.<sup>29</sup> The reaction was followed by measuring the absorbance at 340 nm (SI Figure S8), for 30 minutes after the addition of a stoichiometric amount of ferricyanide. A sample containing L-arginine instead of R<sub>10</sub> was used as control reaction without coacervates present.

We observed a significantly and consistently faster decrease in absorbance at 340 nm for the reaction containing R<sub>10</sub>/3-CM coacervates compared to the control reaction, indicating that NADH oxidation by ferricyanide is enhanced by their accumulation in coacervate droplets. The initial reaction rate ( $v_0$ ) was determined from a linear fit to the first three minutes of the reaction after addition of ferricyanide (SI Figure S9). The initial rate of oxidation of compartmentalized NADH was 1.4 times higher than that of NADH in the control reaction,  $31.8$  and  $23.4 \mu\text{M} \cdot \text{min}^{-1}$ , respectively. The fact that coacervates can increase the rate of redox reactions has been shown before, but has thus far been limited to enzyme driven systems.<sup>42</sup> To verify that the  $v_0$  increase is due to compartmentalization of NADH and not a difference in pH between the coacervates and surrounding solution, the pH was measured over the course of the reaction. For both conditions, the pH slightly dropped during the reaction, but the difference between the phase separated and dilute reaction was never greater than 0.1 (SI Figure S10) These results show that coacervates can sustain and increase NADH oxidation, a process crucial for electron transport

in biology. This is important, as chemical activity would have been essential for protocells and raises the possibility that similar coacervates composed of other metabolites shown in Figure 1 or mixtures of metabolites could have acted as microreactors in a prebiotic environment.

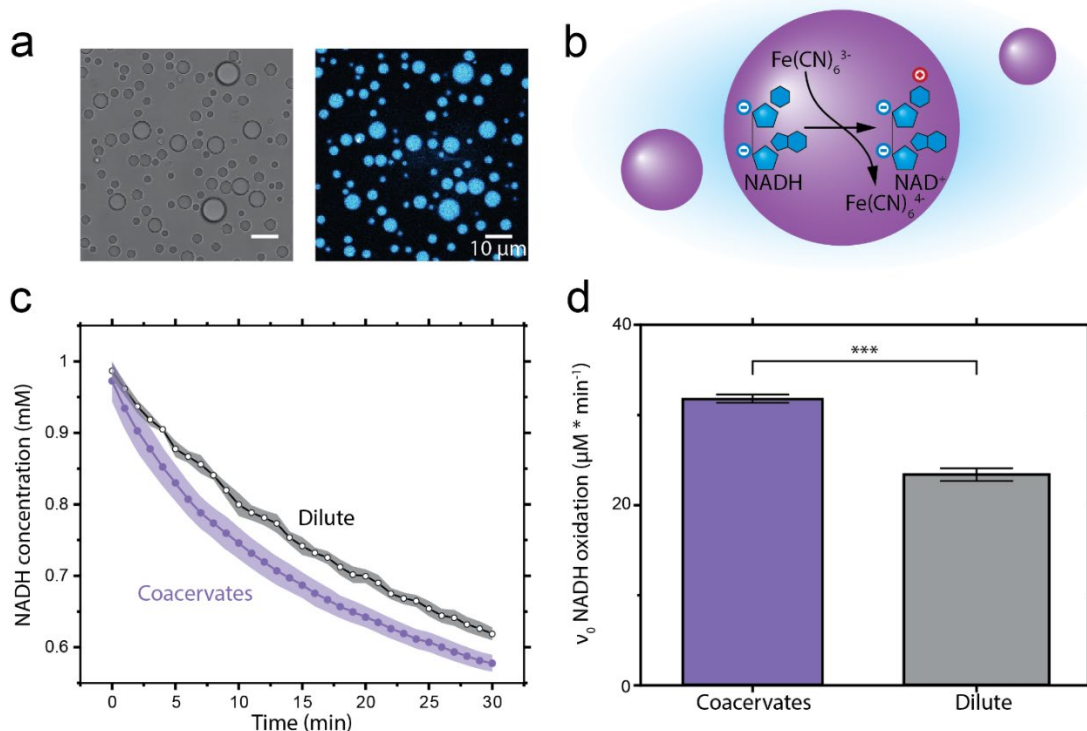


**Figure 3.** Oxidation of NADH is enhanced by coacervate droplets. (a) Microscopy pictures of  $R_{10}/3\text{-CM}$  coacervates containing 1 mM NADH in brightfield (left) and excited with a 405 nm laser (right). (b) NADH oxidation by ferricyanide inside coacervate droplets. (c) Oxidation of NADH by  $\text{Fe}(\text{CN})_6^{3-}$  is increased in the presence of  $R_{10}/3\text{-CM}$  coacervates (purple, filled) compared to the control reaction containing Arg/3-CM (black, open). (d) The initial rate ( $v_0$ ) at which NADH is oxidized is increased in coacervate droplets. Absorbance was measured at 340 nm and a background measurement containing 1mM  $\text{NAD}^+$  and 2 mM ferrocyanide in  $R_{10}/3\text{-CM}$  coacervates or Arg/3-CM was subtracted from the measured data. Shaded regions and error bars represent the standard deviation ( $n = 3$ ).  $v_0$ s are significantly different (\*\*\*) in a two sample  $t$ -test ( $p < 0.001$ ).

### Oxidative decarboxylation of $\alpha$ -keto acids affects stability of coacervate protocells

Finally, having found that coacervates can affect the rate of oxidation of NADH, we wondered whether, vice versa, protometabolic reactions could also affect the coacervate protocells. To this end, we investigated the oxidative decarboxylation of the  $\alpha$ -keto acids isocitroyl formate (**11**) and aconitoyl formate (**12**) to form isocitrate (**13**) and aconitate (**3**), by reacting with hydrogen peroxide (Figure 4a). This reaction leads to loss of a keto group ( $\text{C}=\text{O}$ ), producing anions that are likely to form less stable coacervates with  $R_{10}$  than their precursors (cf. Figure 1). In addition, the carboxylic acid products have a higher  $\text{pK}_a$  than the  $\alpha$ -keto acid substrates and have a slightly lower net charge. And lastly, the oxidative

decarboxylation produces CO<sub>2</sub>, which can dissolve in the aqueous solution and dissociate into bicarbonate and a proton, thereby lowering the pH and increasing the ionic strength of the solution. Since the stability and physicochemical properties of complex coacervates are highly dependent on ionic strength and pH of the solution, such a reaction could significantly affect the nature of the coacervate protocells.<sup>36,43,44</sup>

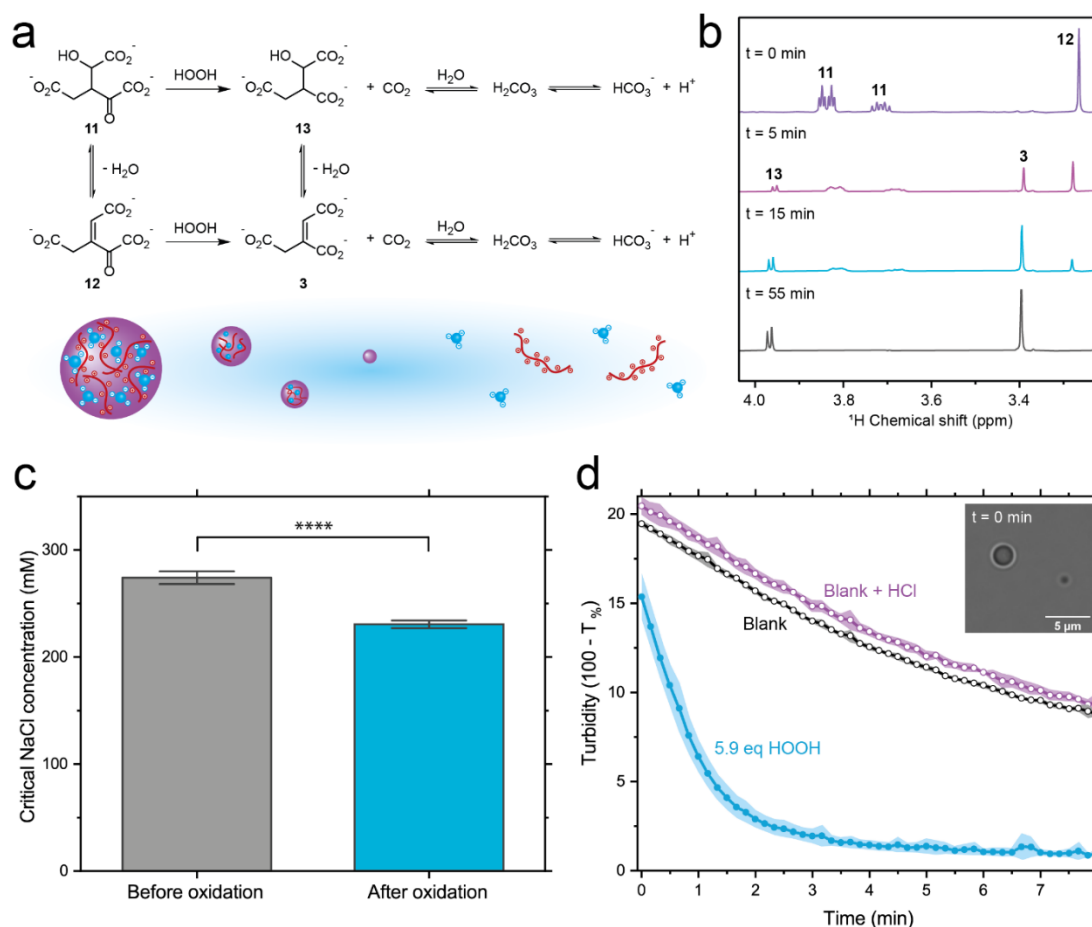


**Figure 4:** Oxidative decarboxylation of isocitroyl formate and aconitoyl formate decreases coacervate stability. (a) Isocitroyl formate (**11**) and aconitoyl formate (**12**) undergo oxidative decarboxylation by hydrogen peroxide (HOOH) to form isocitrate (**13**) and aconitate (**3**), respectively. During the reaction, carbon dioxide is formed, which dissolves in water and decreases the pH due to dissociation into bicarbonate and a proton. (b) Detail of <sup>1</sup>H-NMR spectra over time of the reaction of 15.2 mM isocitroyl formate and 4.1 mM aconitoyl formate with 5.9 equivalents hydrogen peroxide and 1.05 mM 3-(trimethylsilyl)propionic-2,2,3,3-d<sub>4</sub> acid sodium salt internal standard, showing the disappearance of **11** and **12** and the formation of **13** and **3**. The full <sup>1</sup>H-NMR spectra can be found in SI Figure S11. (c) Decrease in critical salt concentration of coacervates made with 15.2 mM isocitroyl formate, 4.1 mM aconitoyl formate and 5 mM R<sub>10</sub> upon oxidation by 5.9 eq hydrogen peroxide. Error bars represent the standard deviation. Critical salt concentrations are significantly different (\*\*\*\*) in a T-test (P < 0.0001). (d) Decrease in turbidity over time upon addition of 3.5 μL 10 wt% (5.9 eq) hydrogen peroxide to coacervates made of 15.2 mM isocitroyl formate, 4.1 mM aconitoyl formate and 5 mM R<sub>10</sub> in the presence of 235 mM sodium chloride. Blanks where the same volume of Milli-Q water and 0.4 mM hydrochloric acid (resulting in a similar decrease in pH as for addition of hydrogen peroxide to water) were added as reference. The standard deviation is depicted as shading around the curves. Insert: Coacervate droplets as observed by Brightfield microscopy.

287 We started by investigating the reaction of 15.2 mM isocitroyl formate and 4.1 mM aconitoyl  
288 formate with 5.9 equivalents hydrogen peroxide in Milli-Q water by  $^1\text{H}$ -NMR spectroscopy (Figure 4b),  
289 and observed that the oxidation reaction is completed in less than one hour, having a similar rate in  
290 absence and presence of  $\text{R}_{10}$  (SI Figure S12). As the reaction progressed, a significant decrease in pH was  
291 measured, starting at 8.42 before the reaction, and decreasing to 6.10 at the end of the reaction (SI Table  
292 S2). Control experiments in which an equal amount of hydrogen peroxide was added to Milli-Q water only  
293 showed a decrease in pH from 6.28 to 5.66 (SI Table S3), indicating that the addition of hydrogen peroxide  
294 alone is not the reason for the significant lowering of pH. Instead, the  $\text{CO}_2$  produced during  
295 decarboxylation of isocitroyl formate and aconitoyl formate partly dissolves and dissociates into  
296 bicarbonate, which causes the decrease in pH.

297 We then investigated what the effect of the reaction is on the stability of the coacervate  
298 protocells. We measured the critical salt concentration of coacervates made of 15.2 mM isocitroyl  
299 formate and 4.1 mM aconitoyl formate with 5 mM  $\text{R}_{10}$ , before and after the reaction with 5.9 equivalents  
300 hydrogen peroxide (Figure 4c), and observed a significant decrease in CSC from  $274.1 \pm 3.2$  mM to  $230.5$   
301  $\pm 2.0$  mM due to the oxidative decarboxylation reaction. Control experiments performed in 100 mM MOPS  
302 buffer (pH 7.55) showed a difference in CSC of 11.8 mM (SI Figure S13), indicating that decreased  
303 coacervate stability can be explained by a combination of decreased interaction strength of the reaction  
304 products, isocitrate / aconitate with  $\text{R}_{10}$ , and the concomitant decrease in pH and increase in ionic strength  
305 due to bicarbonate formation. Such a decrease in CSC and change in composition of the coacervates is  
306 expected to coincide with a change in physicochemical properties of the protocell, including viscosity and  
307 surface tension.<sup>45-47</sup> Moreover, at specific conditions, this protometabolic reaction could be used to  
308 dissolve the compartments in which the reaction is taking place. To test this, we again prepared  
309 coacervate samples made of 15.2 mM isocitroyl formate and 4.1 mM aconitoyl formate with 5 mM  $\text{R}_{10}$ ,  
310 but now added 235 mM NaCl. This value was chosen to be in between the CSCs of the reagents and  
311 products, so that reaction with 5.9 eq hydrogen peroxide would result in dissolution of the coacervates.  
312 We followed the turbidity of the reaction over time by plate reader, and indeed observed a disappearance

of turbidity after 5 minutes (Figure 4d), indicating that the coacervates had fully dissolved. Control experiments where an equivalent amount of Milli-Q water or 0.4 mM HCl (resulting, in pure water, in a similar pH drop as the hydrogen peroxide) was added, only showed a gradual decrease in turbidity due to settling of the coacervate droplets. This shows that metabolic reactions, such as the oxidative decarboxylation of isocitroyl formate and aconitoyl formate, can have a significant effect on the stability of the coacervate protocells, and can even drive their dissolution.

## Conclusions

We have shown that coacervate protocells can form by phase separation of a wide range of prebiotically relevant anionic metabolites with  $R_{10}$ . The difference in electrostatic stability of the metabolite coacervates made with different anions can be explained by the number of interaction sites, such as charged or aromatic groups, and the type of anion. This difference in stability can be exploited to actively form coacervates, for example through the conversion of malonate and glyoxylate to 3-carboxymalate. During this reaction, we observed nucleation and steady growth of coacervate droplets. These metabolite coacervates were able to sustain, and even enhance reactions that were localized to the coacervate interior, such as the oxidation of NADH. We found an increase in oxidation rate by 40%, which we attribute to the high local concentration of NADH and ferricyanide inside the coacervates. Lastly, we have shown that protometabolic reactions can also change physicochemical properties of coacervate protocells, and even decrease their stability such that they dissolve. We used the oxidative decarboxylation of isocitroyl formate and aconitoyl formate by hydrogen peroxide to illustrate this effect, and show that the combination of decreased interaction strength of the reaction products and the decrease in pH due to carbonation of the solution leads to a sufficient lowering of the stability to dissolve the coacervate droplets.

The fact that stable coacervate droplets can be formed from a short polycation and small metabolites with as few as two negative charges is significant, as it offers new insights for the development of protocells with more prebiotically plausible materials. Importantly, the coacervates can be made chemically active with protometabolic reactions that produce or consume droplet material, which opens up possibilities to use the latest insights in prebiotic chemistry to generate liquid

compartments and to link together compartmentalization and metabolism, two central elements of living systems. A scenario in which coacervate protocells nucleate, grow and eventually dissolve with progression of a reaction cycle would be the next step of protocell construction.

## Conflicts of interest

There are no conflicts to declare.

## Acknowledgements

The authors would like to thank Annemiek Slootbeek and Oliver Maguire for useful input and discussions. This project has received funding from the European Research Council (ERC) under the European Union's Horizon 2020 research and innovation programme under grant agreement number 851963. Tiemei Lu acknowledges the China Scholarship Council (CSC) for support.

## References

1. Yewdall, N. A.; Mason, A. F.; Van Hest, J. C. M., The hallmarks of living systems: towards creating artificial cells. *Interface Focus* **2018**, *8* (5), 20180023.
2. Ruiz-Mirazo, K.; Briones, C.; de la Escosura, A., Prebiotic systems chemistry: new perspectives for the origins of life. *Chem Rev* **2014**, *114* (1), 285-366.
3. Gull, M., Prebiotic Phosphorylation Reactions on the Early Earth. *Challenges* **2014**, *5* (2), 193-212.
4. Springsteen, G.; Yerabolu, J. R.; Nelson, J.; Rhea, C. J.; Krishnamurthy, R., Linked cycles of oxidative decarboxylation of glyoxylate as protometabolic analogs of the citric acid cycle. *Nat Commun* **2018**, *9* (1), 91.
5. Stubbs, R. T.; Yadav, M.; Krishnamurthy, R.; Springsteen, G., A plausible metal-free ancestral analogue of the Krebs cycle composed entirely of  $\alpha$ -ketoacids. *Nat Chem* **2020**, *12* (11), 1016-1022.
6. Zhang, X. V.; Martin, S. T., Driving parts of Krebs cycle in reverse through mineral photochemistry. *J Am Chem Soc* **2006**, *128* (50), 16032-3.
7. Muchowska, K. B.; Varma, S. J.; Chevallot-Beroux, E.; Lethuillier-Karl, L.; Li, G.; Moran, J., Metals promote sequences of the reverse Krebs cycle. *Nat Ecol Evol* **2017**, *1* (11), 1716-1721.
8. Muchowska, K. B.; Varma, S. J.; Moran, J., Synthesis and breakdown of universal metabolic precursors promoted by iron. *Nature* **2019**, *569* (7754), 104-107.
9. Basak, S.; Nader, S.; Mansy, S. S., Protometabolic Reduction of NAD(+) with  $\alpha$ -Keto Acids. *JACS Au* **2021**, *1* (4), 371-374.
10. Schrum, J. P.; Zhu, T. F.; Szostak, J. W., The origins of cellular life. *Cold Spring Harb Perspect Biol* **2010**, *2* (9), a002212.
11. Krishnamurthy, R., Giving Rise to Life: Transition from Prebiotic Chemistry to Protobiology. *Acc Chem Res* **2017**, *50* (3), 455-459.
12. Takagi, Y. A.; Nguyen, D. H.; Wexler, T. B.; Goldman, A. D., The Coevolution of Cellularity and Metabolism Following the Origin of Life. *J Mol Evol* **2020**, *88* (7), 598-617.
13. Koga, S.; Williams, D. S.; Perriman, A. W.; Mann, S., Peptide-nucleotide microdroplets as a step towards a membrane-free protocell model. *Nature Chemistry* **2011**, *3* (9), 720-724.
14. Chen, I. A.; Walde, P., From self-assembled vesicles to protocells. *Cold Spring Harb Perspect Biol* **2010**, *2* (7).
15. Monnard, P. A.; Walde, P., Current Ideas about Prebiological Compartmentalization. *Life* **2015**, *5* (2), 1239-63.
16. Hyman, T. A.; Brangwynne, C. P., In Retrospect: The Origin of Life. *Nature* **2012**, *491* (7425), 524-525.
17. van Haren, M. H. I.; Nakashima, K. K.; Spruijt, E., Coacervate-Based Protocells: Integration of Life-Like Properties in a Droplet. *Journal of Systems Chemistry* **2020**, *8*, 107-120.
18. Abbas, M.; Lipiński, W. P.; Wang, J.; Spruijt, E., Peptide-based coacervates as biomimetic protocells. *Chem Soc Rev* **2021**, *50* (6), 3690-3705.

19. Bungenberg de Jong, H. G.; Kruyt, H. R., Coacervation (Partial miscibility in colloid systems). *Proceedings of the Koninklijke Nederlandse Akademie van Wetenschappen* **1929**, (32), 849-856.
20. Brangwynne, C. P.; Tompa, P.; Pappu, R. V., Polymer physics of intracellular phase transitions. *Nature Physics* **2015**, *11* (11), 899-904.
21. Poudyal, R. R.; Guth-Metzler, R. M.; Veenis, A. J.; Frankel, E. A.; Keating, C. D.; Bevilacqua, P. C., Template-directed RNA polymerization and enhanced ribozyme catalysis inside membraneless compartments formed by coacervates. *Nature Communications* **2019**, *10* (1).
22. Abbas, M.; Lipiński, W. P.; Nakashima, K. K.; Huck, W. T. S.; Spruijt, E., A short peptide synthon for liquid-liquid phase separation. *Nat Chem* **2021**, 1046-54.
23. Koga, S.; Williams, D. S.; Perriman, A. W.; Mann, S., Peptide-nucleotide microdroplets as a step towards a membrane-free protocell model. *Nat Chem* **2011**, *3* (9), 720-4.
24. Cakmak, F. P.; Choi, S.; Meyer, M. O.; Bevilacqua, P. C.; Keating, C. D., Prebiotically-relevant low polyion multivalency can improve functionality of membraneless compartments. *Nat Commun* **2020**, *11* (1), 5949.
25. Kim, H.; Jeon, B. J.; Kim, S.; Jho, Y.; Hwang, D. S., Upper Critical Solution Temperature (UCST) Behavior of Coacervate of Cationic Protamine and Multivalent Anions. *Polymers (Basel)* **2019**, *11* (4).
26. Lenton, S.; Hervø-Hansen, S.; Popov, A. M.; Tully, M. D.; Lund, M.; Skepö, M., Impact of Arginine-Phosphate Interactions on the Reentrant Condensation of Disordered Proteins. *Biomacromolecules* **2021**, *22* (4), 1532-1544.
27. Bye, J. W.; Curtis, R. A., Controlling Phase Separation of Lysozyme with Polyvalent Anions. *The Journal of Physical Chemistry B* **2019**, *123* (3), 593-605.
28. Keller, M. A.; Kampjut, D.; Harrison, S. A.; Ralser, M., Sulfate radicals enable a non-enzymatic Krebs cycle precursor. *Nat Ecol Evol* **2017**, *1* (4), 83.
29. Keefe, A. D.; Miller, S. L., Was ferrocyanide a prebiotic reagent? *Orig Life Evol Biosph* **1996**, *26* (2), 111-29.
30. Liu, R.; Orgel, L. E., Polymerization on the rocks: beta-amino acids and arginine. *Orig Life Evol Biosph* **1998**, *28* (3), 245-57.
31. Shakya, A.; King, J. T., DNA Local-Flexibility-Dependent Assembly of Phase-Separated Liquid Droplets. *Biophys J* **2018**, *115* (10), 1840-1847.
32. Mohammadi, P.; Jonkergouw, C.; Beaune, G.; Engelhardt, P.; Kamada, A.; Timonen, J. V. I.; Knowles, T. P. J.; Penttilä, M.; Linder, M. B., Controllable coacervation of recombinantly produced spider silk protein using kosmotropic salts. *J Colloid Interface Sci* **2020**, *560*, 149-160.
33. Spruijt, E.; Westphal, A. H.; Borst, J. W.; Cohen Stuart, M. A.; van der Gucht, J., Binodal compositions of polyelectrolyte complexes. *Macromolecules* **2010**, *43* (15), 6476-6484.
34. Alshareedah, I.; Kaur, T.; Ngo, J.; Seppala, H.; Kounatse, L. D.; Wang, W.; Moosa, M. M.; Banerjee, P. R., Interplay between Short-Range Attraction and Long-Range Repulsion Controls Reentrant Liquid Condensation of Ribonucleoprotein-RNA Complexes. *J Am Chem Soc* **2019**, *141* (37), 14593-14602.
35. Lu, T.; Nakashima, K. K.; Spruijt, E., Temperature-Responsive Peptide-Nucleotide Coacervates. *J Phys Chem B* **2021**, *125* (12), 3080-3091.
36. Nakashima, K. K.; Vibhute, M. A.; Spruijt, E., Biomolecular Chemistry in Liquid Phase Separated Compartments. *Front Mol Biosci* **2019**, *6*, 21.
37. Peeples, W.; Rosen, M. K., Mechanistic dissection of increased enzymatic rate in a phase-separated compartment. *Nat Chem Biol* **2021**, *17* (6), 693-702.
38. Nakashima, K. K.; Baaij, J. F.; Spruijt, E., Reversible generation of coacervate droplets in an enzymatic network. *Soft Matter* **2018**, *14* (3), 361-367.
39. Nakashima, K. K.; van Haren, M. H. I.; André, A. A. M.; Robu, I.; Spruijt, E., Active coacervate droplets are protocells that grow and resist Ostwald ripening. *Nat Commun* **2021**, *12* (1), 3819.
40. Dowler, M. J.; Fuller, W. D.; Orgel, L. E.; Sanchez, R. A., Prebiotic synthesis of propionaldehyde and nicotinamide. *Science* **1970**, *169* (3952), 1320-1.
41. Bonfio, C.; Godino, E.; Corsini, M.; de Biani, F. F.; Guella, G.; Mansy, S. S., Prebiotic iron-sulfur peptide catalysts generate a pH gradient across model membranes of late protocells. *Nature Catalysis* **2018**, *1* (8), 616-623.
42. Ura, T.; Tomita, S.; Shiraki, K., Dynamic behavior of liquid droplets with enzyme compartmentalization triggered by sequential glycolytic enzyme reactions. *Chem Commun (Camb)* **2021**, *57* (93), 12544-12547.
43. van der Gucht, J.; Spruijt, E.; Lemmers, M.; Cohen Stuart, M. A., Polyelectrolyte complexes: bulk phases and colloidal systems. *J Colloid Interface Sci* **2011**, *361* (2), 407-22.
44. Perry, S. L., Phase separation: Bridging polymer physics and biology. *Current Opinion in Colloid & Interface Science* **2019**, *39*, 86-97.
45. Qin, J.; Piftis, D.; Farina, R.; Perry, S. L.; Leon, L.; Whitmer, J.; Hoffmann, K.; Tirrell, M.; De Pablo, J. J., Interfacial tension of polyelectrolyte complex coacervate phases. *ACS Macro Letters* **2014**, *3* (6), 565-568.
46. Liu, Y.; Momani, B.; Winter, H. H.; Perry, S. L., Rheological characterization of liquid-to-solid transitions in bulk polyelectrolyte complexes. *Soft Matter* **2017**, *13* (40), 7332-7340.
47. Spruijt, E.; Sprakel, J.; Stuart, M. A. C.; van der Gucht, J., Interfacial tension between a complex coacervate phase and its coexisting aqueous phase. *Soft Matter* **2010**, *6* (1), 172-178.

## Footnotes

‡ These authors contributed equally.